Degradation of printing ink effluent and industrial predesign by UV/H_2O_2 treatment: A kinetic study

Paula Vitale [a,b,*], Pamela B. Ramos [a,b], Viviana Colasurdo [a,c], Maximiliano I. Delletesse [a,b], Gastón P. Barreto [a,b]

[a] *Universidad Nacional del Centro de la Provincia de Buenos Aires (UNCPBA), Facultad de Ingeniería, INMAT, Av. Del Valle 5737, B7400JWI Olavarría, Argentina*
[b] *CIFICEN, UNCPBA-CONICET-CICPBA, Av. Del Valle 5737, B7400JWI Olavarría, Argentina*
[c] *Instituto Multidisciplinario sobre Ecosistemas y Desarrollo Sustentable, Av. Del Valle 5737, B7400JWI Olavarría, Argentina*

A B S T R A C T

Advanced Oxidation Technologies (AOTs) are effective for treating non-biodegradable organic compounds. AOTs allow to degradation of these pollutants through non-selective attacks by highly reactive radicals. This work studies the reduction of the organic load in real printing ink effluents. The Chemical Oxygen Demand (COD) reduction kinetics was evaluated. The proposed treatment consists of irradiating the effluent in the presence of H_2O_2 with temperature control and commercial UV light lamps (254 nm). Optimal conditions were tested on a pilot scale. The effluents were characterized before and after the treatment. The irradiation, temperature, and oxidizing agent effects were evaluated. The degradations were adjusted to pseudo-first-order kinetics up to 95 % degradations. The optimal k_{deg} was 0.0138 min^{-1} at the laboratory scale (98 % COD reduction in 300 min) and 0.0058 min^{-1} at the pilot scale (90 % COD reduction in 360 min).

The degradation rate increased with temperature. Degradation occurred at a higher rate with mean values of oxidant concentration for all temperatures (between 0.02 and 0.04 mol L^{-1}). The reaction rate increased proportionally to the irradiation, with this effect increasing as the process temperature increased. The pilot prototype was scaled up on an industrial scale, taking into account low-cost and easy-maintenance materials.

1. Introduction

Argentine regulations regarding industrial effluents at the national level (Law 23696, Annex I; Regulatory Decree 999/92, Resolution of National Sanitary Works N° 79179/90) and provincial level (Provincial Water Code of Buenos Aires Law N° 12257, Provincial Resolution of the Ministry of Agrarian Issues and Production N° 336/2003) are stringent. However, the availability of technologies to treat discharges of low biodegradability is deficient. So, alternative treatments are being studied. They include photochemical processes known as Advanced Oxidation Technologies (AOTs) that convert organic pollutants with various chemical structures into lower toxicity and greater biodegradability. AOTs are based on physicochemical processes that produce *in situ* highly reactive transient species with high oxidizing power, such as the hydroxyl radical (HO•), that attack organic pollutants in a non-selective way. These technologies have been widely studied for compounds of low biodegradability at a laboratory scale. Kinetic and mechanistic studies of the degradation of dyes (Kumar et al., 2013, 2018), pharmaceuticals (Quesada-Peñate et al., 2012; Sirtori et al., 2009; Radjenović et al., 2009; Lin and Wu, 2019; Ansarizadeh et al., 2022), pesticides (Malato et al., 2002; Clark et al., 2018; Malakootian et al., 2020), phenols (Suzuki et al., 2015; Vitale et al., 2018; El-Aassar A hameed M, Isawi H, El-Noss M, et al, 2019), colorants (Natarajan et al., 2018; Bergamini et al., 2009; Flores et al., 2014, 2015), additive fuels (Samaei et al., 2016) and many emerging pollutants in isolated form have been developed in simple systems containing only the contaminant in water solution.

Few reports on the degradation kinetics of real effluents in the laboratory (Thanekar and Gogate, 2020; Lu et al., 2022) and pilot-scale (Miklos et al., 2018; Antony et al., 2020; Gautam et al., 2019; Klauck et al., 2017; Pérez Ramos et al., 2019; Papadopoulos et al., 2019; Arslan-Alaton et al., 2021; Ortiz-Marin et al., 2020; Ramos et al., 2020). Real effluents are highly complex systems with many interferences and variables. However, their kinetic information would allow them to scale

* Corresponding author at: Universidad Nacional del Centro de la Provincia de Buenos Aires (UNCPBA), Facultad de Ingeniería, INMAT, Av. Del Valle 5737, B7400JWI Olavarría, Argentina.
E-mail address: pvitale@fio.unicen.edu.ar (P. Vitale).

up the technology to an industrial scale.

Some (laboratory-scale) applications of AOTs have been found to treat landfill leachate (complex matrix with metals in solution and high non-biodegradable organic load). Antony et al. (Antony et al., 2020) propose a zero-valent aluminium-acid system combined with hydrogen peroxide and persulfate for advanced oxidation. The results demonstrate a Chemical Oxygen Demand (COD) reduction of 83 % in 20 min at pH 1.5 and the need to control the concentration of aluminium that rises considerably in the outlet stream. Gautam et al. (Gautam et al., 2019) emphasize electrocoagulation as one of the greenest and cleanest technologies for treating landfill leachate, allowing a COD reduction up to 60 % with a considerable decrease in metal content in the range of 70–90 %. Klauck et al. (Klauck et al., 2017) propose using a hybrid process to stabilize landfill leachate. It consists of the combination of photoelectrooxidation and adsorption with activated carbon, achieving a 62.7 % reduction in COD and a significant toxicity reduction of the effluent. Arslan Alaton et al. (Arslan-Alaton et al., 2021) studied the application of UV-A-assisted iron-based and UV-C-driven oxidation processes as tertiary treatments for the degradation of antibiotics and organic matter present in urban wastewater, achieving reductions of up to 59 % of reduction in dissolved organic carbon. Ortiz-Marin et al. (Ortiz-Marin et al., 2020) studied a sequentially coupled UV/H_2O_2-biologic system to treat an industrial wastewater mixture. AOT removal efficiencies of 49.4 % of COD were achieved after 60 min of irradiation.

Ramos et al. (Ramos et al., 2020) report applying the zero-valent iron Fenton process (at *ca.* neutral native pH) to reduce COD in real textile effluent. The results demonstrate COD reductions of 87 % on a pilot scale, and a treatment plant design applying this technology was proposed. There were two treatment proposals in the bibliography on a laboratory scale regarding printing ink effluents.

Pérez Ramos et al. (Pérez Ramos et al., 2019) propose the application of two AOTs on simulating wastewater: Fenton and electrochemical, obtaining reductions of organic matter of 34 % and 90 %, respectively. Papadopoulos et al. (Papadopoulos et al., 2019) propose treating a real printing ink effluent by electrocoagulation, obtaining COD reductions of 72–85 % in 80 min on an effluent with an initial COD of 9500 $mgO_2\ L^{-1}$.

In a previous work (Vitale et al., 2019), the feasibility of applying different AOTs (UV photolysis, UV/H_2O_2, $Fe°/H_2O_2$, and $UV/H_2O_2/Fe°$) was analyzed at the laboratory scale and through statistical modeling for the reduction of COD in a printing ink effluent. UV/H_2O_2 treatment was demonstrated to be the most suitable process. In this work, a kinetic study of the degradation of real industrial wastewater by UV/H_2O_2 process and industrial equipment pre-design was carried out to continue these studies. The studied effluent was obtained from a graphic company characterized in previous work (Vitale et al., 2019). This company produces multi-wall paper containers for various industrial and commercial uses (cement, lime, flour, fertilizers, milk powder, tea, and dry chemicals, among other products). Raw materials are papers, plastics, aluminized coils, adhesives, and inks. The paper sacks are manufactured in two stages. The first one consists of printing the paper, which is carried out by a flexographic process. In the second stage, the paper is folded into tubes, closed, and reinforced at the bottom end, with a small opening or valve in one corner at the top.

Depending on the colors necessary, the printing line can be one to ten printing units, including different types of finishes such as varnishes, plastic lamination, and film stamping. The production varies from the type of packaging, designs, colors used, and size and seasonality of the lots. This influences the type of effluent obtained, its composition, and organic load. The liquid effluent is generated by cleaning the ink trays. Trays are washed when the machines change ink (after a production batch is finished) or on scheduled cleaning days by a batch process, generating variable effluent volumes (discontinuously). The average volume of effluent generated daily is 1 m³, with a sludge production of 590 kg per day. The effluent treatment currently has a duration of 48 h and is efficient only in the removal of solids. This treated effluent does not meet the requirements established by Argentine regulations regarding high organic load limits (*ca.* 15,000 $mgO_2\ L^{-1}$ of COD) for land discharge and low biodegradability ($BOD_5/COD = 0.06$).

This work involved a kinetic study of the degradation of printing ink effluent by UV/H_2O_2 process and industrial equipment pre-design. The novelty of this work consists of the kinetic study of a real system of great complexity and unknown composition, providing useful design parameters for subsequent engineering projects. The system studied consists of a non-biodegradable wastewater sample in a printing ink industry dedicated to printing paper packaging. The selection of the best AOT treatment was evaluated in previous work (Vitale et al., 2019). It involves a combination of UV light irradiation (254 nm) in the presence of H_2O_2 as an oxidant. The present work studied the kinetic aspects, the effects of temperature, oxidant concentration, radiation intensity, and activation parameters. A pilot-scale experience was also carried out to obtain scalable parameters later at an industrial level. A pre-design of industrial scale-up equipment was made.

2. Materials and methods

2.1. Sampling

Samples were taken randomly to determine the parameters established by the legislation and their variability. The effluent was centrifuged to remove the solids, then characterized. The sampling and characterization performed before and after treatment were carried out using the previously reported methodology (Vitale et al., 2019). COD was determined by SM 5220 D (closed reflux digestion method, colorimetric (APHA, 2017).

Parameters of interest were obtained for each sample and are mentioned in each section of the work. The initial values for the main parameters were in the following ranges COD: 11000–22400 $mgO_2\ L^{-1}$; pH: 6.49 – 6.83 and non-biodegradable (BOD_5/COD *ca.* 0.06).

2.2. Experimental setup

Lab-scale experiments were performed in a 50 mL batch photoreactor placed in a thermostatically controlled water bath (15 ± 2 ˚C) inside an aluminium tray that reflected UV light. An array of five commercially available 6 W germicidal lamps (wavelength 254 nm) with independent power switches irradiated the samples from above. The aluminuim tray size allowed up to 10 experimental runs to be carried out simultaneously under the same irradiation and temperature conditions (Fig. 1a). 50 mL of effluent was added to the photoreactor in a typical test. It was allowed to rest for about 15 min, and then the degradation reaction was started by adding the oxidant (H_2O_2, between 0 and 0.08 M) and turning the lamps on simultaneously.

The laboratory photoreactor was reconfigured to conduct the pilot experiment under the same irradiation conditions (Fig. 1b). This design considered the available space and existing structures in the target industry for subsequent scaling.

The aluminium tray used as the water bath at the lab scale was used as the reactor at the pilot scale. The recirculation system consisted of an external container (3 L), where the oxidant was injected, the system was heated, and connected to the tray (2 L) where the irradiation occurred. Considering the possibilities of industrial design, this division of the treated volume was considered. First, direct irradiation on a flat plate would avoid using fragile and expensive materials such as quartz and simplify the safety issues to consider. Secondly, it was taken into account that since the space available for the industrial scale is small, it is not possible to irradiate the total volume of liquid simultaneously. So, a proportion is set: 40 % of the total volume will be irradiated in a system with complete recirculation. The oxidant was added to the system shortly before starting the experimental run, allowing for the homogenization of the concentration. The experiment began when the lamps were turned on.
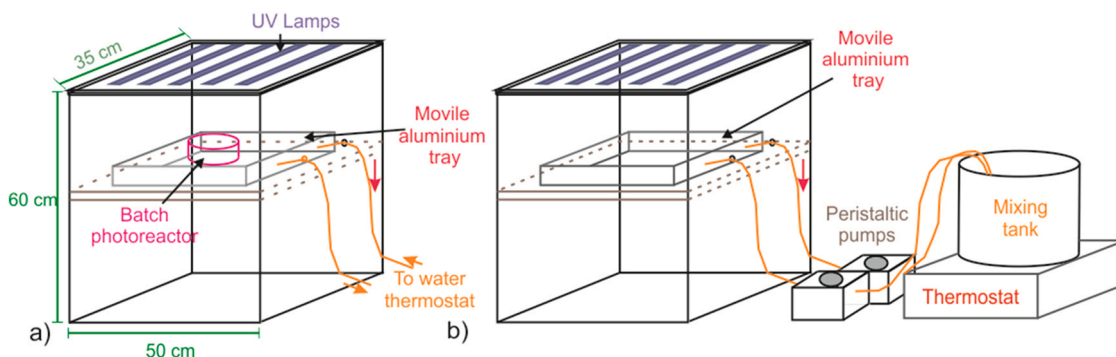
Fig. 1. Schematic diagram of a) Equipment used for the laboratory tests and b) adaptation used for the pilot test.

The commercial germicidal lamps used in the device were characterized by focusing the light input to a monochromator (Acton Research Corporation, Model 504) in Czerny-Turner configuration with a quartz lens of 40 mm diameter and 200 mm focal length and an optical path of 50 cm. The dispersion is produced by a reflection diffraction grating of 1200 lines mm^{-1}. The scattered light is detected at the output of the monochromator by a non-intensified silicon diode array (Princeton Instrument Inc., Model RY-1024, PDA). Emission spectra were produced with centers at different wavelengths to verify that they did not have significant emission peaks at wavelengths other than 254 nm. The emission lines of the lamps were characteristic of mercury throughout the spectrum, obtaining the highest emission intensity at 253.65 nm. In the area around 480 nm, no lines were detected. Around 510 nm, the I line of Hg can be observed again (253.65 nm) in the second diffraction order.

The UV light intensity was measured by chemical actinometry to determine the incidence of light inside the photoreactor. This technique is based on a chemical photodegradation compound with a well-known quantum yield (at a specific wavelength). In this way, measuring the reaction rate allowed us to determine the absorption rate of photons (Pérez-Estrada, 2003). The chemical actinometer used in this work was hydrogen peroxide, whose quantum yield is φ = 0.5 mol Einstein^{-1} at 254 nm (Nicole et al., 1990). First, the lamps inside the black box were turned on for half an hour to measure the radiation intensity until the compartment reached the steady-state conditions (*ca.* 30 °C). Then the lamps were turned off, and the reactor was placed inside the box with 50 mL of H$_2$O$_2$ (the experiment was carried out in triplicate). The lamps were turned on again, and then time was started (t = 0). The concentration of the oxidizing agent in the reactor was measured at different times using visible UV- spectrophotometry, using a quartz cuvette, and measuring the absorbance at 220 nm. The total time of the actinometry measurement was 160 min.

The actinometry results obtained for 1, 2, 3, 4, and 5 lamps are shown in Fig. 2a. The radiation intensity varied linearly with the number of lamps (Fig. 2b). The intensity can be considered a continuous variable. The measurements covered part of the lamps with aluminium foil to represent a non-whole number of lamps, and the intensity adjustment was linear.

The UV intensity I expressed in Einstein s^{-1} corresponds to the tests in 50 mL reactors (irradiation surface 78.5 cm^2). The photon flux density (PFD, Einstein m^{-2} s^{-1}) can be calculated by dividing the intensity by the irradiation surface to make the calculations independent of the reactor area and know the equivalent intensity for the pilot scale tests.

2.3. Kinetic studies of COD removal

The global degradation kinetics was monitored by measuring COD (SM5220D) and the pH at different times. In a typical experimental run, the pH was measured, and small portions of effluent (0.2 mL) were collected every hour to prepare the appropriate dilution and determine COD. The percentage degradation of the oxidizable material (*%D*) was analyzed from the data obtained by Eq. 1:

$$\%D = 100 - \left(\frac{[COD]_t}{[COD]_0} \times 100 \right) \tag{1}$$

The degradation kinetics were determined by the integral method assuming an overall reaction order 1, and the ln ([COD]$_t$/[COD]$_0$) *vs.* t was plotted, where [COD] were the obtained concentrations of chemical oxygen demand in mg O$_2$ L^{-1}. The system would correspond to a pseudo-first-order reaction; therefore, the data of each run was adjusted with a straight line, obtaining the global degradation rate constant (k$_{deg}$) from its slope. The effect of temperature on the values of the
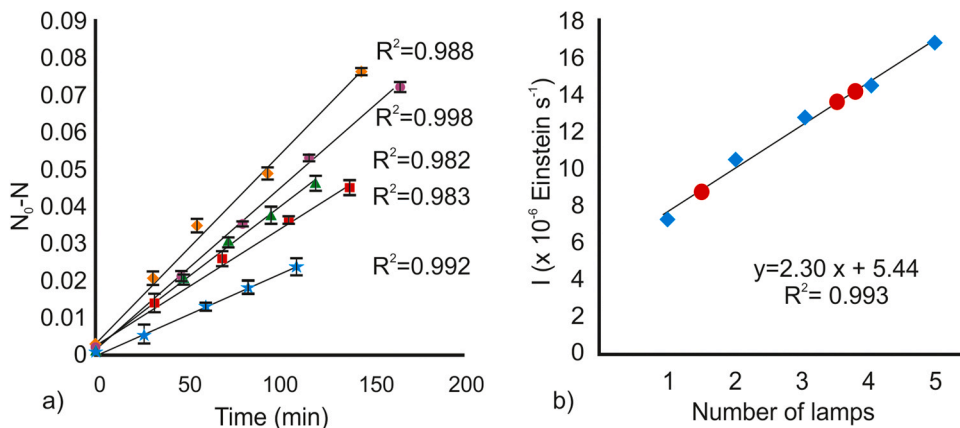

Fig. 2. Actinometry. a) Difference of actinometer moles (N-N$_0$) in time for 1 (★), 2 (■), 3 (▲), 4 (●), and 5 (◆) lamps switched on. b) Representation of UV intensity according to the number of lamps switched on (◆), and with part of the lamp covered up (●).
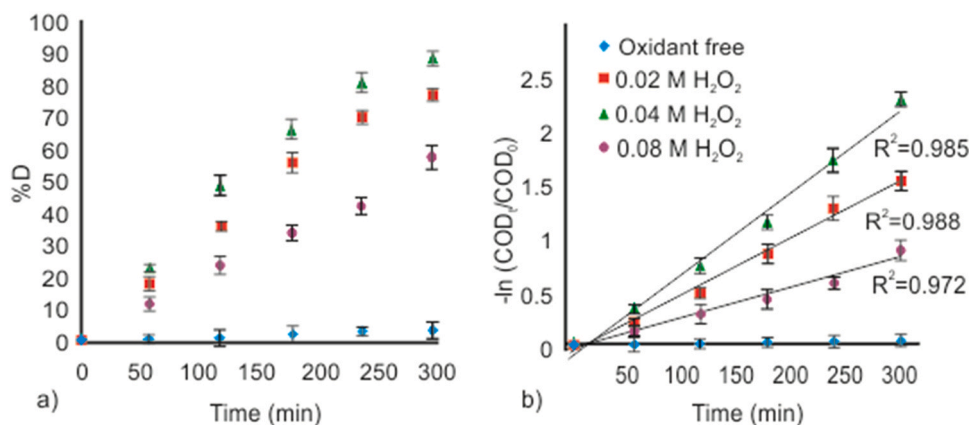
Fig. 3. a) Percentage of COD reduction as a function of time (45 °C and radiation of 1.04×10^{-5} Einstein s^{-1}) with different oxidant concentrations. b) Graphical representation of pseudo first-order kinetics at 45 °C and 1.04×10^{-5} Einstein s^{-1} radiation with the respective linear correlation coefficients.

Table 1

Values of the pseudo first-order reaction rate constants were determined for different H_2O_2 concentrations and 1.04×10^{-5} Einstein s^{-1} radiation intensity.

$[H_2O_2]$ (mol L^{-1})	$k_{deg\ (15\ °C)}$ x10^3 min^{-1}	$k_{deg\ (30\ °C)}$ x10^3 min^{-1}	$k_{deg\ (45\ °C)}$ x10^3 min^{-1}
0.02	4.35	5.17	5.22
0.04	5.67	6.64	7.49
0.08	1.08	1.95	2.71

degradation rate constant (k_{deg}) can be represented by the Arrhenius equation (Eqs. 2 and 3):

$$k_{deg} = A \times e^{\frac{-E_a}{RT}} \tag{2}$$

$$ln(k_{deg}) = ln(A) - \frac{E_a}{R}\left(\frac{1}{T}\right) \tag{3}$$

where k_{deg} is the degradation rate constant of the effluent, T is the absolute temperature, A is the pre-exponential factor, E_a is the activation energy, and R is the universal gas constant (R = 8.3143 J mol^{-1}K^{-1}). The error corresponding to the activation energy was determined by the method described by Huyberechts (Huyberechts et al., 1955). Errors were calculated from the values of the rate constants of the degradation reaction (obtained experimentally, at least in duplicate in all cases) and the temperatures expressed in Kelvin.

3. Results and discussion

3.1. Kinetic study of COD removal

The degradation reaction was evaluated by measuring COD and pH to determine the isolated effects of each factor and the activation parameters. The kinetics were measured over 300 min. The reduction of the organic load of the effluents was obtained by varying one parameter at a time.

Degradation kinetics were obtained at temperatures of 15 °C, 30 °C and 45 °C (kinetics at 15 °C and 30 °C are shown on support material). Fig. 3a shows the variation of the COD over time for different oxidant concentrations between 0 and 0.08 mol L^{-1}, maintaining the intensity of UV radiation at 1.04×10^{-5} Einstein s^{-1}, while Fig. 3b shows a linearized plot of the pseudo first-order kinetics ln(CODt/COD0) *versus* t. In all cases where oxidant was added, the kinetics were adjusted with R$^2 > 0.9$, considered a good fit for a real system (Cheng et al., 2014). Data fits were

made to check for other reaction orders, and no-good fits were obtained. For the experiment carried out without oxidant, the degradations obtained were so low (*ca.* 3 %) that it is not adequate to establish a reaction order.

Table 1 presents the values of the rate constants obtained for different oxidant concentrations and temperatures.

Fig. 4a and b, show the variation of COD percentage over time for different radiations between 0 and 1.67×10^{-5} Einstein s^{-1} and a linearized representation of the pseudo-first-order kinetics of a typical degradation model (ln (COD$_t$/COD$_0$) *vs.* t) are shown, respectively. The figures present the kinetics performed at 45 °C (also conducted at 15 and 30 °C, shown in Supporting information). The degradations were adjusted to pseudo-first-order kinetics up to 95 % degradations.

Table 2 shows the reaction rate constants obtained at different irradiances and temperatures. An oxidant concentration of 0.04 mol L^{-1} of H_2O_2 was maintained in all cases.

The best results were obtained for high temperature and irradiation values (45 °C and 1.67×10^{-5} Einstein s^{-1}) and average oxidant values (0.04 mol L^{-1}). The maximum degradation brought in the kinetic study allowed a COD removal of 98.6 % in 300 min to an initial COD of 18200 mg O_2 L^{-1}.

The bibliography does not report kinetic or degradation data achieved for real effluents from the graphic industry applying UV/H_2O_2. Therefore, these results are compared with those obtained by Papadopoulus et al. (Papadopoulos et al., 2019) using another AOT (electrocoagulation) for the same type of effluent. In that work, an 80 % reduction of COD was obtained in 80 min, with an initial COD 5000 mgO$_2$ L^{-1}. A 70 % reduction in COD was achieved in the present study in 60 min with an initial COD 3.6 times higher. However, it is necessary to prolong the treatment time to reach COD values compatible with the legislation (< 500 mgO$_2$ L^{-1}).

3.2. Oxidant effects

Fig. 5a shows the degradation (%D) (measured as COD removal) achieved in the effluent after 300 min of treatment, depending on the oxidant concentration.

The most significant degradations were obtained for intermediate concentrations of H_2O_2 (between 0.02 and 0.04 mol L^{-1}). Initially, increasing the dose of H_2O_2 increased the production of HO• available to break down the organic molecules, causing a decrease in the residual COD of the treated effluent. However, the degradation was disfavored by adding an oxidant, probably because the H_2O_2 consumes the HO• to form a less reactive radical HO$_2$• (Feng et al., 2010).

The pH variation as a function of time for different oxidant concentrations added at 45 °C is shown in Fig. 5b, while Fig. 5c shows the pH obtained at 300 min as a function of oxidant concentration for different temperatures.
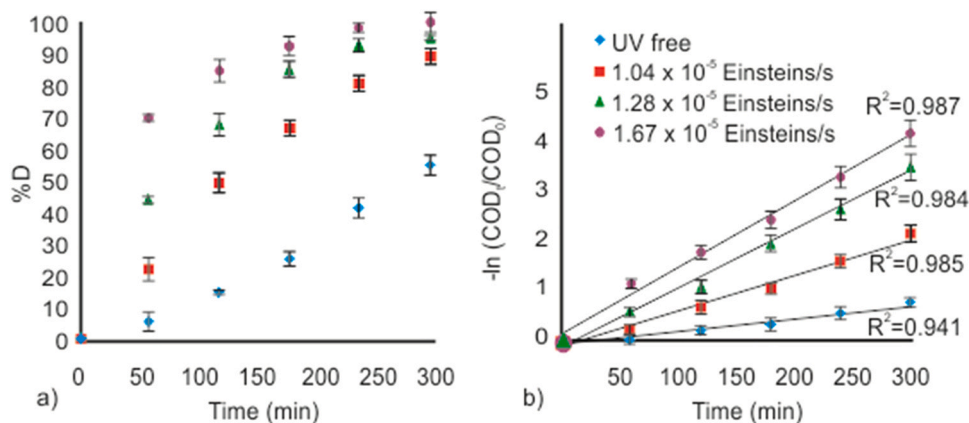
Fig. 4. a) %D as a function of time, and b) Graphical representation of pseudo first-order kinetics at 45 °C with an H_2O_2 concentration of 0.04 mol L^{-1} with the respective linear correlation coefficients.

Table 2
Values of the pseudo first-order reaction rate constants were determined for different radiations and an H_2O_2 concentration of 0.04 mol L^{-1}.

Radiation UV Einstein s^{-1}	$k_{deg\ (15\ °C)}$ x10^3 min^{-1}	$k_{deg\ (30\ °C)}$ x10^3 min^{-1}	$k_{deg\ (45\ °C)}$ x10^3 min^{-1}
0	2.26	2.23	2.63
1.04×10^{-5}	5.67	6.64	7.49
1.28×10^{-5}	6.15	8.51	13.00
1.67×10^{-5}	6.37	9.00	13.76

In Fig. 5b, it can be observed that pH increases throughout the reaction. However, the final pH (at 300 min) is lower as the oxidant concentration increases (Fig. 5c). This is probably because an increase in the amount of HO• makes the medium more oxidizing, degrading organic species to their more oxidized forms (organic acids, for example) (Blesa, 2001). The observed pH effect is opposite to that reported by other authors, in experiments carried out on simplified systems (distilled water, pollutants) (Domènech et al., 2001).

It was counteracting the unexpected increase in pH, as described by Hamad et al. (Hamad et al., 2014), in the degradation of polyvinyl alcohol in water by the H_2O_2 process. The authors associated it with the consumption of the acid species formed in the oxidative mechanisms. In this experiment, the initial pH of the effluent was *ca.* 6.49, and the pH variation during the treatment ranged between 1.93 and 0.92 pH units. The final pH in all cases was very close to neutrality or slightly alkaline. The decreased pH with increasing H_2O_2 levels was less than one pH unit at all the studied temperatures.

The increase in pH during effluent degradation may be due to matrix effects. An increase in the hardness and total alkalinity of the system was detected, mainly associated with calcium bicarbonates in the solution. The alkalinity doubled during an optimal treatment, and the total hardness increased several times when the maximum degradations were obtained.

Ghodbane et al. (Ghodbane and Hamdaoui, 2010) reported for the degradation of Acid Blue 25 by UV/H_2O_2, the presence of bicarbonates reduces the efficiency of the process since HO• radicals are consumed in the formation of carbonates (Eq. 4). This could explain the increase in the alkalinity of the system and consequently the pH.

$$HCO_3^- + HO^\bullet \rightarrow H_2O + CO_3^{\bullet-} \tag{4}$$

Table 1 presents the variation of the global rate constants (k_{deg}) for the degradation kinetics as a function of the oxidant added to the system. It can be observed that for all temperatures and with radiation of 3.7×10^{-2} Einstein s^{-1}, the degradation occurred at a higher rate for average values of oxidant concentration (between 0.02 and 0.04 mol L^{-1}). The highest %D in Fig. 5a can be seen within the same H_2O_2 concentration range in line with this trend.

3.3. UV radiation effects

Fig. 6a shows the % reduction COD in the effluent after treatment (300 min) with an oxidant concentration of 0.04 mol L^{-1}.

Greater degradation levels were observed as the radiation intensified, mainly due to the formation of HO• through the photolysis of the oxidant (Hamad et al., 2014; Ghodbane and Hamdaoui, 2010; Litter, 2005). By increasing the irradiation, there is a decrease in the final COD percentage due to an increase in photons up to 1.28×10^{-5} Einstein s^{-1}. An increase in radiation intensity from 1.28×10^{-5} to 1.67×10^{-5} Einstein s^{-1} for all temperatures did not significantly increase in %D (ANOVA, Tukey's test, $p < 0.05$). The complete degradation of the effluent under study was achieved under experimental conditions of 1.28×10^{-5} Einstein s^{-1} and 45 °C.

Table 2 shows the variation of the global rate constants (k_{deg}) for the degradation kinetics as a function of UV radiation and system temperature. It can be seen that the reaction rate increases proportionally to UV radiation, with this effect increasing with temperature up to radiation of 1.28×10^{-5} Einstein s^{-1}.

The effect of temperature on k_{deg} was not significant between 30 and 45 °C (ANOVA, Tukey's test $p < 0.05$) up to 1.04×10^{-5} Einstein s^{-1}, and beyond that, radiation intensity heating produces higher degradation rates.

No significant effect was observed on the irradiated systems' final pH (300 min). There are appreciable differences in the final pH between the irradiated and non-irradiated systems (Fig. 6b and c).

3.4. Temperature effects

The oxidant concentration effect on the %D of the effluent for a fixed irradiance of 1.04×10^{-5} Einstein s^{-1} (Fig. 5a) and the irradiation effect for a constant oxidant concentration 0.04 mol L^{-1} (Fig. 6a) was evaluated as a function of temperature. There was an increase in the %D of the treated effluent in both cases as the temperature increased. It was also observed (Table 2) that temperature increase had no effect when no oxidant was added (the degradation reached *ca.* 3 %). The effect of the oxidant on the final pH for constant irradiation is shown in Fig. 5c. It can be seen that the final pH increased at higher temperatures. This effect was also present for stable peroxide concentrations and irradiation variation (Fig. 6c).

The effect of oxidant concentration on k_{deg} for a fixed radiation intensity (1.04×10^{-5} Einstein s^{-1}, Table 1) and the irradiation effect for a fixed oxidant amount of 0.04 mol L^{-1} are shown for different temperatures (Table 2). It can be observed that the degradation rate increased with temperature and that the temperature effect increased with UV radiation. The trend observed in all the effects analyzed in isolation is similar to that of the model proposed by (Vitale et al., 2019) with an experimental design.
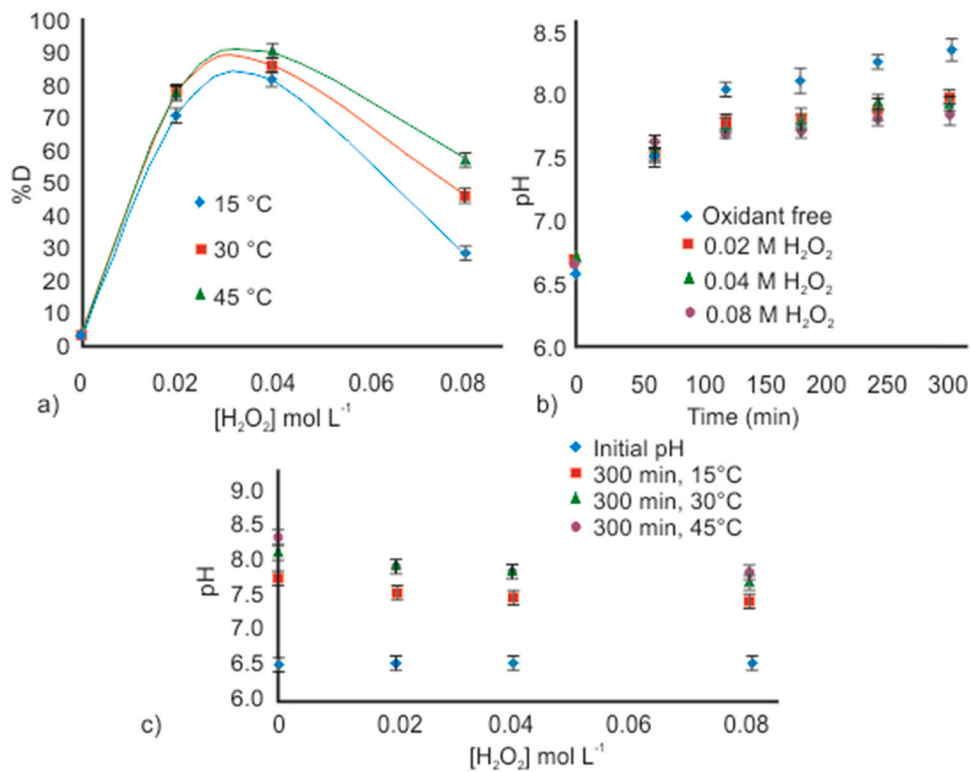
Fig. 5. Effect of the oxidant concentration (at constant UV irradiation, 1.04×10^{-5} Einstein s^{-1}) a) on %D at 300 min for different temperatures; b) on pH over time (at 45 °C); c) on final pH for different temperatures (at 300 min).
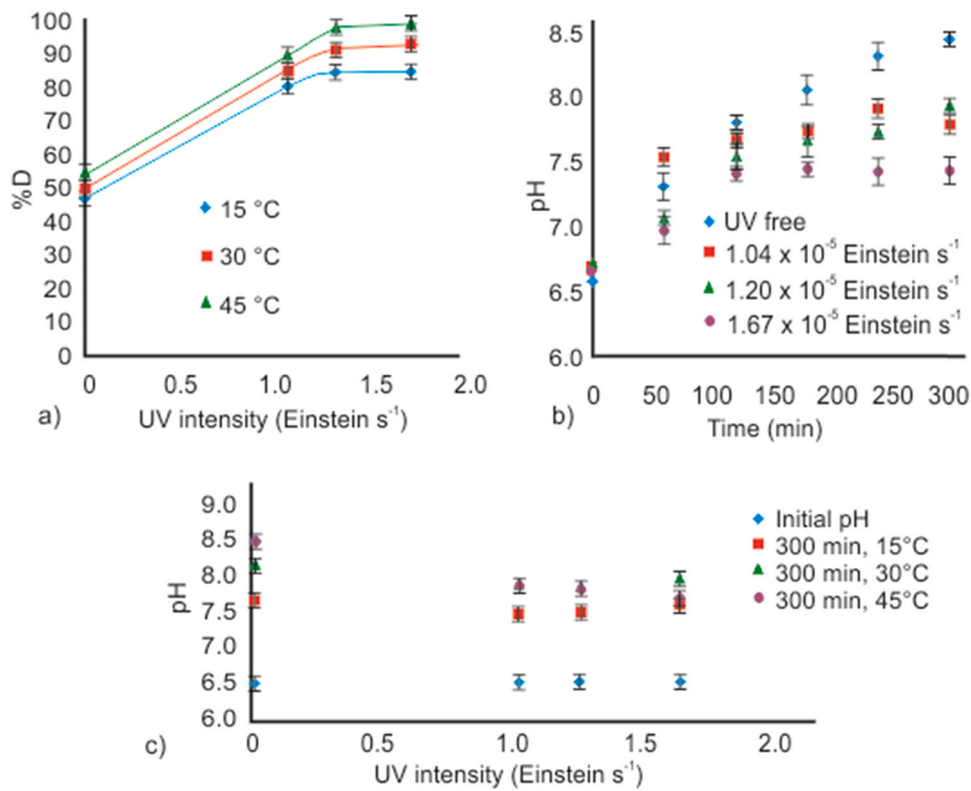

Fig. 6. Effect of UV radiation (at constant H_2O_2 concentration, 0.04 M): a) on %D at 300 min for different temperatures; b) on pH over time (at 45 °C); c) on final pH for different temperatures (at 300 min).

Table 3
Activation parameters for tested conditions.

H_2O_2 (mol L^{-1})	UV intensity (x10^5 Einstein s^{-1})	Arrhenius equation	
		A	Ea (kJ mol^{-1})
0.04	UV free	< 0.001	3.71
0.02	1.04	0.001	4.71
0.04	1.04	0.002	7.08
0.08	1.04	0.334	23.46
0.04	1.28	0.275	18.97
0.04	**1.67**	**0.361**	**19.52**

3.5. Determination of the activation parameters

This work did not study the degradation reaction mechanism on a single compound. The activation parameters corresponded to a complex system and were determined with the following considerations:

- The COD of the effluent was approached as a parameter to measure the global concentration of the organic material.
- Degradation rate constants correspond to a global rate.
- The purpose of determining the values of the activation parameters has a process-design interest, especially considering that it is the degradation reaction of organic pollutants of a real effluent.

The effect of temperature on k_{deg} (for the studied kinetics that gave the most favourable results, 0.040.04 mol L^{-1-1} of H_2O_2 and radiation of $1.67 \times 101.67 \times 10^{-5-5}$ Einstein s^{-1-1}, PFD = 2,13 x 102,13$\times 10^{-4-4}$ Einstein m^{-2-2} s^{-1-1}, Table 3) can be represented by the Arrhenius equation (Eq. 3). The graphical representation of this equation (R^2 = 0.9924) allows obtaining the activation energy value for the determining stage of the process rate (E$_a$ = 19.52 ± 1.22 kJ mol^{-1}).

E$_a$ increased with increasing H_2O_2 concentrations for the same radiation intensity. The same effect was found when irradiation was raised for a constant oxidant concentration.

3.6. Pilot-scale test

The optimal operating conditions obtained through the model and verified by the laboratory experiment were then tested on a pilot scale (2.13×10^{-4} Einstein m^{-2} s^{-1}, 45 °C, and 0.04 mol L^{-1} concentration of H_2O_2). A total volume of 5 L was treated in a complete recirculation batch system. The irradiation tray contained 2 L of liquid, and the other 3 L were placed in an external tank, where the system was heated. Two reciprocating pumps set the circulation rate from the tank to the tray at 0.5 L min^{-1}.

The degradation results over time are shown in Fig. 7 (adjusted to pseudo-first-order kinetics).

A degradation of *ca.* 78 % was obtained at 300 min (COD is reduced from 22,400 mg O$_2$ L^{-1} to 4900 mgO$_2$ L^{-1}), which is a good value considering that only 2 of the 5 L were under irradiation at any time. With one more hour of treatment, it was possible to achieve over 90 % degradation (COD: 2030 mgO$_2$ L^{-1}). The obtained kinetic equation estimated that it would take 655 min to reach the COD value for discharge (500 mgO$_2$ L^{-1}). The biodegradability of the treated water did not change (BOD$_5$ /COD = 0.06), so a biological process could not be coupled to improve the efficiency of the treatment. The treatment efficiency at the pilot scale concerning the lab-scale results was 79.36 % (300 min).

The rate constant obtained for the kinetics at 2.13×10^{-4} Einstein m^{-2} s^{-1}, 45 °C, and 0.04 mol L^{-1} concentration of H_2O_2 (k$_{deg}$ = 0.0058 min^{-1} at pilot scale) is approximately two-fifths of that achieved at laboratory scale (k$_{deg}$ = 0.0138 min^{-1}), with this proportion being similar to that of the irradiated volumes. This could indicate that the generated radical reactions end after the irradiation ends.

The literature does not report kinetic or pilot scale studies on real effluents from the printing industry applied UV/H$_2$O$_2$. This work is of great importance since the results obtained are necessary for designing effluent treatments on an industrial scale.

The experiments carried out by Thuy et al. (2020) (Thuy et al., 2021) on the application of electrocoagulation for the treatment of printing wastewater at a pilot scale report COD reductions of 81.9 % (initial COD 2511 mgO$_2$. L^{-1}). They also agree that the COD reductions of the pilot scale are slightly lower than those of the laboratory scale. These results are comparable to UV/H$_2$O$_2$ treatment on a pilot scale.

3.7. Industrial pre-design

A pre-design is carried out on an industrial scale to treat 1 m^3 of printing ink effluent per day, with an initial COD similar to the 22400 mgO$_2$ L^{-1} pilot-scale test stripped of solids by a previous primary process. Since the operation of the industrial plant is batch type, it is proposed that the treatment process is also batch. The goal of treatment is to obtain an outlet COD of less than 500 mgO$_2$ L^{-1}.

3.7.1. Construction materials, safety conditions, and proposed geometry

The construction of a rectangular aluminium tray of suitable dimensions is proposed. The tray will have a capacity of 400 L of liquid (keeping the proportion of volume irradiated in pilot-scale). In said tray, irradiation will be carried out employing an arrangement of UV lamps (254 nm) placed in the upper part fitted with parabolic mirrors that allow UV light to be reflected and concentrated in the area tray. This arrangement provides irradiation to be carried out directly,
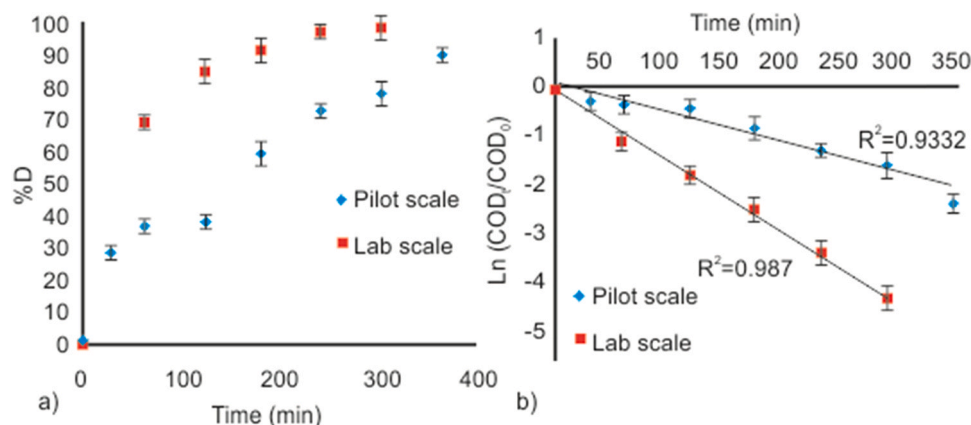
Fig. 7. Degradation results under optimal conditions at pilot and laboratory scales. a) % degradation, and b) pseudo-first-order kinetics of the pilot test.
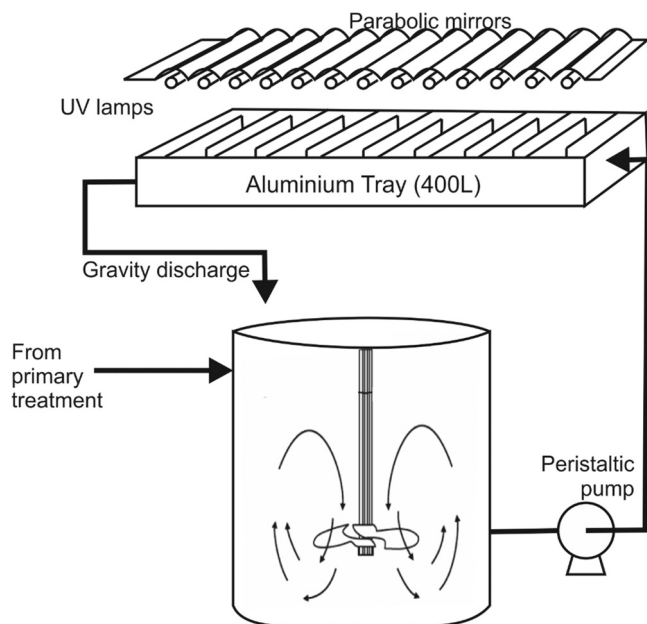
Fig. 8. Representative arrangement of equipment on an industrial scale.

avoiding the use of high-cost and fragile construction materials that allow the passage of UV light, such as quartz used in systems where the lamps are submerged. It also notably reduces the staining of materials and dirt that prevents the passage of light. The liquid is in continuous movement and will be recirculated from and to a mixing tank (1 m³ of total capacity) containing 600 L of liquid during the process. The equipment arrangement is shown in Fig. 8.

The tray must be covered to prevent the entry of materials from outside into the system. It must be protected from the side to avoid UV radiation that may affect the personnel performing the tasks. This protection must be removable to ensure the dry cleaning of the tray (with brushes) and the replacement/repair of the lamp system.

3.7.2. Irradiation tray/mixing tank sizing

The aluminium tray (400 L) must be supported on a suitable structure for weight and vibrations. It must guarantee UV light penetration; for this reason, the height of the liquid must be small (in drinking water, the UV transmittance is 70–98 % at 254 nm along 1 cm (Wright and Cairns, 1998). Good mixing must be ensured to guarantee the irradiation of all the liquid.

A liquid depth of 10 cm is set, so the tray should have an area of 4.00 m² (3.20 m x 1.25 m, which is suggested to be divided into two sections of 1.60 m x 1.25 m). The tray is fitted with a system of baffles similar to a contact chamber to ensure the mixing and homogenizing of the liquid's residence time in the system.

For the contact chamber to have good efficiency, the length/width (L/W) ratio of each channel should be taken as high as possible. An L/

W > 40/1 ratio is necessary to achieve maximum hydraulic performance with a flow of characteristics close to ideal (Dalhammar et al., 2014). Thus, 52 deflectors (by tray section) were needed, leaving 3.1 cm wide passage channels. The tray is discharged through an overflow channel to control the height of the liquid.

The mixing tank is cylindrical with a capacity of 1 m³ to store all the effluent to be processed. However, during the process, it must only contain 600 L, with a stirring system that guarantees the homogenization of the liquid; in this tank, the oxidant necessary for the process is added.

3.7.2.1. Design parameters for the irradiation system. The optimal PFD in the pilot-scale process was 2.13×10^{-4} Einstein m^{-2} s^{-1} (5.95×10^{-5} Einstein s^{-1}). Since one mole of photons per second (1 Einstein s^{-1}) at 254 nm is equivalent to 471 kJ of energy (Tian et al., 2020), the energy received by the system was calculated as 2.81×10^{-2} kW. When the energy efficiency of UV lamps was assumed to be 25 % (Bolton et al., 2001), the power of energy input (P) was 0.112 kW.

Electric energy per mass (E_{EM}) is the electric energy in kilowatt-hours [kWh] required to bring about the degradation of a unit mass (*e.g.*, 1 kg of O$_2$ COD equivalent) of a contaminant C in polluted water. E_{EM} was calculated using Eq. 5 proposed by Bolton et al. (Bolton et al., 2001) for batch systems.

$$E_{EM} = \frac{P}{V} \quad \frac{t}{(\gamma_i - \gamma_f)} \quad 10^6 \tag{5}$$

E_{EM} value was in kWh/kg, P was the rated power of the system [kW], V was the volume [L] of water treated in the time t [h], γ was the mass concentration [mg L^{-1}] of pollutant.

For the pilot-scale photoreactor, E_{EM} was 10.25 KWh Kg^{-1}.

This E_{EM} value should be the same on an industrial scale if the geometry is similar to that used on a pilot scale. So, the power of the system to industrial scale (P_{IS}) value was obtained, taking into account a 10-hour treatment: $P_{IS} = 22.45$ kW (power of energy input to reactor, P = 5.61 kW).

This power was represented by a UV intensity 1.19×10^{-2} Einstein s^{-1} (PDF= 2.97×10^{-3} Einstein m^{-2} s^{-1}) that affects the system through the irradiation tray. The final number of lamps in the array will depend on the photon intensity of the commercially available type of lamp, considering that the relationship between the number of lamps and the intensity is linear, as shown in Fig. 2a.

3.7.3. Estimation of necessary reagents and dosage

For 1 m³ treatment, adding 2.13 L of oxidant (250 vol, commercial quality) is necessary. The oxidant can be added in two pulses to guarantee availability throughout the process, taking into account the duration of the process and the agitation in the mixing tank.

3.7.4. Liquid circulation/ recirculation pump

The use of a peristaltic pump was considered since the liquid is not in contact with the mechanical parts of the equipment, reducing groves associated with materials and avoiding corrosion (highly oxidizing environment). A discharge rate of 0.66 m s^{-1} was chosen, which was

Table 4
Equipment Costs.

Equipment	US$	Observation
Mixing Tank	3500	Market cost (Argentine) of a 1 m³ PVC tank with agitation
Aluminium Tray	4055	Estimated by material calculation (5 mm thick aluminium sheets - Total tray and defectors area 20 m²)
Irradiation system	2650	Estimated by material calculation (5 mm thick anodized aluminium sheets – Total Area = 6 m²)
UV Lamps	16840	Estimated cost based on power according to the market price of germicidal lamps (USD / W = 0.75)
Peristaltic Pump	1100	Market cost (Argentine)
Pipes	4500	Estimated as 30 % of the cost of the equipment.
Total	**32645**	

Table 5
Operation Costs.

Operative Cost	USD/m³ effluent	Reference
UV Irradiation	6.52	This work
Heating	0.34	(Ortiz-Marin et al., 2020)
Reagets	25.06	(Ortiz-Marin et al., 2020)
Total Operative Costs	31.92	

optimal in the laboratory test to prevent splashing the lamps and fouling.

The flow rate was determined for mixing to ensure complete mixing (turbulent flow in a channel with a rectangular section, hydraulic diameter 0.054 m; Re > 4000). Considering that effluent properties are similar to water, a minimum operating flow guaranteed complete mixing was $0.05 \, \mathrm{m \, s^{-1}}$. This value was considerably lower than the proposed discharge rate ($0.66 \, \mathrm{m \, s^{-1}}$), and the whole mixture was assured. The total effluent volume passed through the tray twice in 10 h (whit $0.2 \, \mathrm{m^3 h^{-1}}$). The final average travel length of the tray was 133.2 m, and the residence time of the liquid was 2.05 h.

3.8. Costs estimation

Table 4 shows the estimated equipment costs for constructing the arrangement shown in Fig. 8. Table 5 shows the operating costs previously reported in Vitale et al., 2019 (Vitale et al., 2019). The charge referred to irradiation has been updated based on the necessary Power (P_{IS}) obtained in this work.

Regarding the production costs for the treatment of effluents from the printing industry, two aspects should be considered: first, UV/H_2O_2 technology has been reported as advantageous for colorant and pigment removal, obtaining high efficiencies in general (Ortiz-Marin et al., 2020; Yang et al., 1998). Secondly, the order of total costs based on kg COD removed was considered. Literature reports that UV/H_2O_2 processes have been economically more viable than other treatment options: against O_3, O_3/UV and O_3/UV/H_2O_2 process for the acetate and polyester fiber dyeing effluent based on COD removal (Azbar et al., 2004); Babaei et al. report that UV/H_2O_2 is a more economical option than UV/Fe^{2+}/H_2O_2, UV/percarbonate/Fe^{2+} or UV/percarbonate process for petrochemical effluents (Babaei and Ghanbari, 2016).

4. Conclusions

Under the optimal experimental conditions obtained with the proposed model, degradations of 98.22 % ± 0.96 % at 300 min of reaction at laboratory scale and *ca.* 90 % at 360 min at the pilot-scale (where two-fifths of the treated effluent were irradiated) were reached. A time of 11.3 h of treatment was estimated for a 98 % degradation, which is considered a time of industrial interest, considering that the current process takes 48 h. The overall degradation process was favoured at higher temperatures. The kinetics of degradation by UV/H_2O_2 were adjusted to a pseudo-first-order up to 90 % conversions, obtaining a rate constant of $k_{deg} = 0.0138 \, \mathrm{min^{-1}}$ for the best degradations. The activation energy was also determined ($E_a = 19.52 \, \mathrm{kJ \, mol^{-1}}$).

The work presents a complete study of applying an advanced oxidation process to a real industrial effluent. Applying this process (UV/H_2O_2) on a pilot scale allows for obtaining final discharge parameters following the legislation and projecting a scaling that can be carried out at an industrial level for daily batch treatment of 1 m³. Also, the application allows considering relatively low-cost materials and simple geometries. This industrial-scale arrangement anticipates an equipment expense of approximately US$ 33000 and a production cost of about US$ 32 per m³.

Data Availability

Data will be made available on request.

Declaration of Competing Interest

The authors declare that they have no known competing financial interests or personal relationships that could have appeared to influence the work reported in this paper.

Appendix A. Supporting information

Supplementary data associated with this article can be found in the online version at doi:10.1016/j.clwas.2023.100106.

References

Ansarizadeh, M., Tabatabaei, T., Samaei, M.R., et al., 2022. Modelling of cefixime (CFIX) removal using photocatalyst/UV/polyurethane by response surface methodology (RSM): optimisation and kinetic study. Int. J. Environ. Anal. Chem. 102, 8075–8091. https://doi.org/10.1080/03067319.2020.1843650

Antony, J., Niveditha, S.V., Gandhimathi, R., et al., 2020. Stabilized landfill leachate treatment by zero valent aluminium-acid system combined with hydrogen peroxide and persulfate based advanced oxidation process. Waste Manag. 106, 1–11. https://doi.org/10.1016/j.wasman.2020.03.005

APHA, AWWA, WPCF (2017) Estándar Methods for the examination of wáter and weaster., APHA. U.S.A.

Arslan-Alaton, I., Karatas, A., Pehlivan, Ö., et al., 2021. Effect of UV-A-assisted iron-based and UV-C-driven oxidation processes on organic matter and antibiotic resistance removal in tertiary treated urban wastewater. Catal. Today 361, 152–158. https://doi.org/10.1016/j.cattod.2020.02.037

Azbar, N., Yonar, T., Kestioglu, K., 2004. Comparison of various advanced oxidation processes and chemical treatment methods for COD and color removal from a polyester and acetate fiber dyeing effluent. Chemosphere 55, 35–43. https://doi.org/10.1016/j.chemosphere.2003.10.046

Babaei, A.A., Ghanbari, F., 2016. COD removal from petrochemical wastewater by UV/hydrogen peroxide, UV/persulfate and UV/percarbonate: Biodegradability improvement and cost evaluation. J. Water Reuse Desalin. 6, 484–494. https://doi.org/10.2166/wrd.2016.188

Bergamini, R.B.M., Azevedo, E.B., Araújo, L.R.R., De, 2009. Heterogeneous photocatalytic degradation of reactive dyes in aqueous TiO₂ suspensions: decolorization kinetics. Chem. Eng. J. 149, 215–220. https://doi.org/10.1016/j.cej.2008.10.019

Blesa M.A. (2001) Eliminación de Contaminantes por Fotocatálisis Heterogénea, Red CYTED. La Plata.

Bolton J.R., Bircher K.G., Tumas W., Tolman C.A. (2001) Figures-of-merit for the technical development and application of advanced oxidation technologies for both electric- and solar-driven systems.

Cheng, H., Chou, S., Chen, S., Yu, C., 2014. Photoassisted Fenton degradation of phthalocyanine dyes from wastewater of printing industry using Fe(II)/γ-Al₂O₃ catalyst in up-flow fluidized-bed. 1307–12. J. Environ. Sci. (China) 26. https://doi.org/10.1016/S1001-0742(13)60604-X

Clark, K.K., Mezyk, S.P., Abbott, A., Kiddle, J.J., 2018. Kinetic studies of the AOP radical-based oxidative and reductive destruction of pesticides and model compounds in water. Chemosphere 197, 193–199. https://doi.org/10.1016/j.chemosphere.2017.12.190

Dalhammar, C., Machacek, E., Bundgaard, A., et al., 2014. Addressing resource efficiency through the Ecodesign Directive: A review of opportunities and barriers.

Domènech, X., Jardim, W.F., Litter, M.I., 2001. Capitulo 1: procesos avanzados de oxidación para la eliminación de contaminantes. In: Blesa, M.A. (Ed.), Programa iberoamericano de ciencia y tecnología para el desarrollo (CYTED), CYTED. La Plata, pp. 3–25.

El-Aassar A hameed M, Isawi H, El-Noss M, et al, 2019. Design and fabrication of continuous flow photoreactor using semiconductor oxides for degradation of organic pollutants. J. Water Process Eng. 32. https://doi.org/10.1016/j.jwpe.2019.100922

Feng, F., Xu, Z., Li, X., et al., 2010. Advanced treatment of dyeing wastewater towards reuse by the combined Fenton oxidation and membrane bioreactor process. J. Environ. Sci. 22, 1657–1665. https://doi.org/10.1016/S1001-0742(09)60303-X

Flores, A., Nesprias, K., Vitale, P., et al., 2014. Heterogeneous photocatalytic discoloration/degradation of rhodamine B with H_2O_2 and spinel copper ferrite magnetic nanoparticles. Aust. J. Chem. 67. https://doi.org/10.1071/CH13435

Flores, A., Vitale, P., Eyler, G.N., Cañizo, A.I., 2015. Remoción de colorantes textiles aplicando procesos fotoquímicos oxidativos (UV/H_2O_2 /lana de acero comercial). Afinidad LXXII 188–195.

Gautam, P., Kumar, S., Lokhandwala, S., 2019. Advanced oxidation processes for treatment of leachate from hazardous waste landfill: a critical review. J. Clean. Prod. 237, 117639. https://doi.org/10.1016/j.jclepro.2019.117639

Ghodbane, H., Hamdaoui, O., 2010. Decolorization of antraquinonic dye, C.I. Acid Blue 25, in aqueous solution by direct UV irradiation, UV/H_2O_2 and UV/Fe(II) processes. Chem. Eng. J. 160, 226–231. https://doi.org/10.1016/j.cej.2010.03.049

Hamad, D., Mehrvar, M., Dhib, R., 2014. Experimental study of polyvinyl alcohol degradation in aqueous solution by UV/H_2O_2 process. Polym. Degrad. Stab. 103, 75–82. https://doi.org/10.1016/j.polymdegradstab.2014.02.018

Huyberechts, M.S., Halleux, A., Kruys, P., 1955. Une application de Calcul Statistique à la Cinétique Chimique. Bull. Des. Sociétés Chim. Belg. 64, 203–209. https://doi.org/10.1002/bscb.19550640502

Klauck, C.R., Giacobbo, A., Altenhofen, C.G., et al., 2017. Toxicity elimination of landfill leachate by hybrid processing of advanced oxidation process and adsorption. Environ. Technol. Innov. 8, 246–255. https://doi.org/10.1016/j.eti.2017.07.006

Kumar, M.S., Sonawane, S.H., Bhanvase, B.A., Bethi, B., 2018. Journal of Water Process Engineering Treatment of ternary dye wastewater by hydrodynamic cavitation combined with other advanced oxidation processes (AOP's). J. Water Process. Eng. 23, 250–256. https://doi.org/10.1016/j.jwpe.2018.04.004

Kumar, P., Agnihotri, R., Mondal, M.K., 2013. Catalytic treatment of synthetic dye wastewater: COD and color reduction. J. Environ. Chem. Eng. 1, 440–447. https://doi.org/10.1016/j.jece.2013.06.008

Lin, C., Wu, M., 2019. Journal of Water Process Engineering Performance of a large reactor in degrading sulfamethazine in water using UV and persulfate. J. Water Process Eng. 31, 100874. https://doi.org/10.1016/j.jwpe.2019.100874

Litter M.I. (2005) Tecnologías avanzadas de oxidación: tecnologías solares. In: Blesa MA, Blanco Galvez J (eds) Solar safe water, cost effective solar photocatalytic technology to water decontamination and disinfection in rural areas of developing countries, Red Iberoa. San Martin, Buenos Aires, pp 73–90.

Lu, J., Zhuo, Q., Ren, X., et al., 2022. Treatment of wastewater from adhesive-producing industries by electrocoagulation and electrochemical oxidation. Process Saf. Environ. Prot. 157, 527–536. https://doi.org/10.1016/j.psep.2021.10.035

Malakootian, M., Shahesmaeili, A., Faraji, M., et al., 2020. Advanced oxidation processes for the removal of organophosphorus pesticides in aqueous matrices: a systematic review and meta-analysis. Process Saf. Environ. Prot. 134, 292–307. https://doi.org/10.1016/j.psep.2019.12.004

Malato, S., Blanco, J., Vidal, A., Richter, C., 2002. Photocatalysis with solar energy at a pilot-plant scale: an overview. Appl. Catal. B 37, 1–15. https://doi.org/10.1016/S0926-3373(01)00315-0

Miklos, D.B., Hartl, R., Michel, P., et al., 2018. UV/H_2O_2 process stability and pilot-scale validation for trace organic chemical removal from wastewater treatment plant effluents. Water Res. 136, 169–179. https://doi.org/10.1016/j.watres.2018.02.044

Natarajan, S., Bajaj, H.C., Tayade, R.J., 2018. Recent advances based on the synergetic effect of adsorption for removal of dyes from waste water using photocatalytic process. J. Environ. Sci. (China) 65, 201–222. https://doi.org/10.1016/j.jes.2017.03.011

Nicole, I., De Laat, J., Dore, M., et al., 1990. Use of U.V. radiation in water treatment: measurement of photonic flux by hydrogen peroxide actinometry. Water Res 24, 157–168.

Ortiz-Marin, A.D., Amabilis-Sosa, L.E., Bandala, E.R., et al., 2020. Using sequentially coupled UV/H2O2-biologic systems to treat industrial wastewater with high carbon and nitrogen contents. Process Saf. Environ. Prot. 137, 192–199. https://doi.org/10.1016/j.psep.2020.02.020

Papadopoulos, K.P., Argyriou, R., Economou, C.N., et al., 2019. Treatment of printing ink wastewater using electrocoagulation. J. Environ. Manag. 237, 442–448. https://doi.org/10.1016/j.jenvman.2019.02.080

Pérez Ramos, J.M., Pereira-queiroz, N.M., Santos, D.H.S., et al., 2019. Printing ink effluent remediation: a comparison between electrochemical and Fenton treatments. J. Water Process Eng. 31. https://doi.org/10.1016/j.jwpe.2019.100803

Pérez-Estrada L.A. (2003) Determinación de la eficiencia de tres concentradores solares utilizados en la degradación fotocatalítica de contaminantes disueltos en agua. Tesis de Maestría, Universidad de Sonora.

Quesada-Peñate, I., Julcour-Lebigue, C., Jáuregui-Haza, U.J., et al., 2012. Degradation of paracetamol by catalytic wet air oxidation and sequential adsorption - Catalytic wet air oxidation on activated carbons. J. Hazard Mater. 221–222, 131–138. https://doi.org/10.1016/j.jhazmat.2012.04.021

Radjenović, J., Sirtori, C., Petrović, M., et al., 2009. Solar photocatalytic degradation of persistent pharmaceuticals at pilot-scale: Kinetics and characterization of major intermediate products. Appl. Catal. B 89, 255–264. https://doi.org/10.1016/j.apcatb.2009.02.013

Ramos, P.B., Vitale, P., Barreto, G.P., et al., 2020. Treatment of real non-biodegradable wastewater: feasibility analysis of a zero-valent iron/H_2O_2 process. J. Environ. Chem. Eng. 8, 103954. https://doi.org/10.1016/j.jece.2020.103954

Samaei M.R., Maleknia H., Azhdarpoor A. (2016) A comparative study of removal of methyl tertiary-butyl ether (MTBE) from aquatic environments through advanced oxidation methods of H2O2/nZVI, H2O2/nZVI/ultrasound, and H2O2/nZVI/UV. Desalination Water Treat 57:21417–21427. https://doi.org/10.1080/19443994.2015.1123193.

Sirtori, C., Zapata, A., Oller, I., et al., 2009. Decontamination industrial pharmaceutical wastewater by combining solar photo-Fenton and biological treatment. Water Res 43, 661–668. https://doi.org/10.1016/j.watres.2008.11.013

Suzuki, H., Araki, S., Yamamoto, H., 2015. Evaluation of advanced oxidation processes (AOP) using O_3, UV, and TiO_2 for the degradation of phenol in water. J. Water Process Eng. 7, 54–60. https://doi.org/10.1016/j.jwpe.2015.04.011

Thanekar P., Gogate P.R. (2020) Improved processes involving hydrodynamic cavitation and oxidants for treatment of real industrial effluent. Sep Purif Technol Accepted M: https://doi.org/10.1016/j.seppur.2020.116563.

Thuy, N.T., Hoan, N.X., Van Thanh, D., et al., 2021. Application of electrocoagulation for printing wastewater treatment: from laboratory to pilot scale. J. Electrochem. Sci. Technol. 12, 21–32. https://doi.org/10.33961/jecst.2019.00444

Tian, F.X., Ye, W.K., Xu, B., et al., 2020. Comparison of UV-induced AOPs (UV/Cl_2, UV/NH_2Cl, UV/ClO_2 and UV/H_2O_2) in the degradation of iopamidol: kinetics, energy requirements and DBPs-related toxicity in sequential disinfection processes. Chem. Eng. J. 398, 125570. https://doi.org/10.1016/j.cej.2020.125570

Vitale, P., Cañizo, A.I., Eyler, G.N., 2018. Degradation of phenol assisted by spinel cooper ferrites and residual magnetic materials. Afinidad 75, 212–221.

Vitale, P., Ramos, P.B., Colasurdo, V., et al., 2019. Treatment of real wastewater from the graphic industry using advanced oxidation technologies: Degradation models and feasibility analysis. J. Clean. Prod. 206, https://doi.org/10.1016/j.jclepro.2018.09.105

Wright H.B., Cairns W.L. (1998) Ultraviolet Ligth.

Yang, Y., Wyatt, D.T., Bahorsky, M., 1998. Decolorization of dyes using UV/H_2O_2 photochemical oxidation. Text. Chem. Color. 30, 27–35.